Journal of Porous Media 13(1), 1–11 (2010)

ANISOTROPIC DIFFUSION IN FIBROUS POROUS MEDIA

Yoshito Nakashima & Susumu Kamiya*

National Institute of Advanced Industrial Science and Technology (AIST), Central 7, Higashi 1-1-1, Tsukuba, Ibaraki 305-8567, Japan

*Address all corespondence to Yoshito Nakashima E-mail:nakashima.yoshito@aist.go.jp

Original Manuscript Submitted: 6/17/2008; Final Draft Received: 11/30/2008

Some porous media possess fibrous structures. Examples include the geologically deformed porous rocks, white matter in human brain tissue, and fiber-reinforced composite materials. These anisotropic porous media show strong diffusive anisotropy. This study focused on a system consisting of randomly placed parallel rods as a model of fibrous porous media, and describes the analysis of three-dimensional diffusive anisotropy through the lattice random walk computer simulations. The rods were completely impermeable, and nonsorbing random walkers migrate in the percolated pore space between the parallel rods. Direction-dependent self-diffusivity was calculated by taking the time derivative of the mean square displacement of the walkers, and its three-dimensional shape was expressed graphically as a shell-like object by polar representation. Systematic simulations for varied rod packing densities revealed that the shell-like object was no longer convex ellipsoidal, but was constricted in the direction normal to the rod axis when the maximum-to-minimum diffusivity ratio of the diffusion ellipsoids exceeded 1.5 (i.e., when the rod volume fraction exceeded 34 vol %). An analytical solution of the direction-dependent self-diffusivity with constriction is presented for the lattice walk along a straight pore. The solution suggests that the ellipsoid constriction observed for the randomly placed parallel rods is a remnant of the anisotropic pore structure of the hexagonal closest packing, which is the end member of the rod packing. The onset condition of the constriction of the shape of the direction-dependent self-diffusivity is investigated analytically using a diffusion tensor expression. The analysis reveals that the constriction occurs when the maximum-to-minimum diffusivity ratio exceeds exactly 1.5, which agrees well with the simulation results. The critical value of 1.5 can also be applicable to the geologically deformed natural porous rocks having more complex pore structure compared with the simple rod packing system.

KEY WORDS: *anisotropy, diffusion ellipsoid, diffusion tensor, diffusion weighted MRI*

1. INTRODUCTION

Diffusion through a pore space is an important transport mode in porous media with small Péclet numbers. The solid framework of some porous media possesses fibrous structures. Examples include the geologically deformed (elongated) pumice rocks (Nakashima et al., 2008), human nervous system (Frank, 2002), and fiber-reinforced composite materials (Guild and Summerscales, 1993; Teshima et al., 2001). Because trajectories of random walkers in the pore space are restricted by the anisotropic solid framework, the resultant diffusivity of the walkers also is anisotropic. Thus, direction-dependent diffusivity can be analyzed quantitatively for such anisotropic porous media. This study focused on a system consisting of computer-generated, randomly placed, parallel impermeable rods as a model of fibrous porous media, and involves 3D lattice random walk simulations of nonsorbing walkers in the anisotropic discrete pore space between the parallel rods to calculate the walkers' mean square displace-

1091-028X/10/$35.00

NOMENCLATURE

$\boldsymbol{D}$	diffusion tensor of rank 2
D_x	normalized diffusivity in the x direction
D_{xy}	normalized diffusivity averaged on the $x-y$ plane
D_z	normalized diffusivity in the z direction
$\boldsymbol{u}$	unit vector
ℓ	dimension of a cubic voxel of the three-dimensional image system
n	number of random walkers
x, y, z	Cartesian coordinate
$\langle x(\tau)^2\rangle$, $\langle y(\tau)^2\rangle$, $\langle z(\tau)^2\rangle$	mean square displacement of walkers along the x-, y-, and z-axis, respectively

Greek Symbols

α	coordinate for the projection of random walk trajectories
$\langle\alpha(\tau)^2\rangle$	mean square displacement of walkers along the α-axis
$\langle\alpha(\tau)^2\rangle_{\mathrm{free}}$	$\langle\alpha(\tau)^2\rangle$ for the lattice walk in free space
δ	complementary angle of θ (radians)
ε	volume fraction of solid rods in the porous system (vol %)
θ, ϕ	polar coordinate (deg)
τ	dimensionless integer time

ment along an arbitrary direction in 3D space. Direction-dependent diffusivity was calculated by calculating the time derivative of the directional mean square displacement, and expressed graphically as a shell-like 3D object by polar representation. Extensive simulations were conducted by systematically varying rod packing density, and the effects of packing density on the 3D shape of the shell-like object were analyzed thoroughly.

Particular attention was paid to the unusual shape, namely, constriction of the direction-dependent diffusivity. Previous studies have suggested that a polar representation of the direction-dependent diffusivity for highly anisotropic fibrous porous media is no longer convex ellipsoidal, but is constricted in the direction of minimum diffusivity for nervous systems (Frank, 2002) and for pumice rocks (Nakashima et al., 2008). The present simulation study reveals that the constriction of the direction-dependent self-diffusivity also occurred for the randomly packed parallel rod system, a very simple model system compared with nervous and rock systems. Although there are studies on the anisotropic diffusion in fibrous porous media (e.g., Frank, 2002; Sen and Basser, 2005; Jian et al., 2007; Fieremans et al., 2008), few studies exist on the systematic and quantitative analysis of the constriction of the 3D shape of the direction-dependent self-diffusivity. To understand the nature of the constriction, an exact solution of the direction-dependent self-diffusivity with constriction was presented for the lattice walk in a straight pore. The onset mechanism of the constriction of the prolate shape of the direction-dependent self-diffusivity was investigated analytically using a diffusion tensor expression.

2. CALCULATION OF AN ANISOTROPIC DIFFUSIVITY FOR A RANDOMLY PACKED ROD SYSTEM

The method for calculating an anisotropic self-diffusivity by 3D lattice random walk in the pore space is outlined. The lattice random walk algorithm is useful for analysis of 3D diffusion in discrete or digitized porous media (Nakashima and Watanabe, 2002; Nakashima et al., 2004). A lattice walk Mathematica program (DellipsoidM6.nb) was developed to calculate the anisotropic diffusivity. The following is only an outline of the method; for further information about subjects such as the lattice walk algorithm and data processing of DellipsoidM6.nb, refer to Nakashima and Kamiya (2007) and Nakashima et al. (2008).

As a model of fibrous porous media, 3D digital images of randomly placed parallel rods were computer generated by the random sequential packing algorithm (Tanemura, 1988). The image system consists of parallel solid rods with infinite length and finite uniform diameter. Each rod was placed randomly and sequentially if it did not overlap any rods already placed. If a rod overlapped any rods already placed, the rod was removed and a new trial was conducted. An example of the discrete image system

consisting of numerous cubic voxels is shown in Fig. 1a. The image system is characterized by a single parameter: volume fraction of the rods, ε. Rods are completely impermeable, and nonsorbing random walkers migrate in the percolated pore space between the parallel rods. Owing to the blocky nature of discrete images, too small rod diameter values are undesirable to approximate the smooth outline of rods. Too large diameter values are unacceptable to complete long-distance diffusion simulations in a reasonable time. After some trial and error, we found that several tens of voxels are suitable. Three values (19, 37, and 73 voxels) were employed as the rod diameter to confirm independence of the calculated diffusivity from the diameter value.

The random walk simulation should be performed only in a percolated pore cluster responsible for macroscopic or long-distance transport of materials (not in isolated small pores). An example of such undesirable isolated pore surrounded by rods is shown in Fig. 1b. Thus, the raw 3D images generated by random sequential packing need to be preprocessed by cluster labeling (Ikeda et al., 2000; Nakashima and Kamiya, 2007) to exclude isolated pores and to extract a single percolated pore cluster. Fortunately, we confirmed that the influence of isolated pores was almost negligible owing to their small volume fraction values. For example, the volume fraction of all isolated pore clusters was as small as 0.033 vol %, while that for the single percolated pore cluster was 45.970 vol %, even for a densely packed system of $\varepsilon = 53.997$ vol %. This demonstrates that almost all of the pores are connected to form a single large pore cluster responsible for long-distance diffusive transport. However, cluster labeling preprocessing was applied to all of the rod image systems to maximize the accuracy of the simulations.

The program DellipsoidM6.nb executes the nonsorbing 3D lattice walk on a percolated pore cluster in a simple cubic lattice image system with a periodic boundary condition using a mirror operation (Nakashima et al., 2008). Because self-diffusion is assumed, neither chemical gradient nor macroscopic diffusive flux exists. The starting position of the random walk was chosen randomly from among the voxels of the percolated pore cluster. An excellent pseudorandom number generator, Mersenne Twister, developed by Matsumoto and Nishimura (1998) was implemented in DellipsoidM6.nb. The random walker should be nonsorbing because its purpose is calculation of the geometrical tortuosity of the pore structure, and undesirable sorption of walkers on the solid surface should be eliminated.

Before the simulation of the rod system, the nonsorbing lattice random walk through the percolated pore cluster by DellipsoidM6.nb was performed for the 3D image

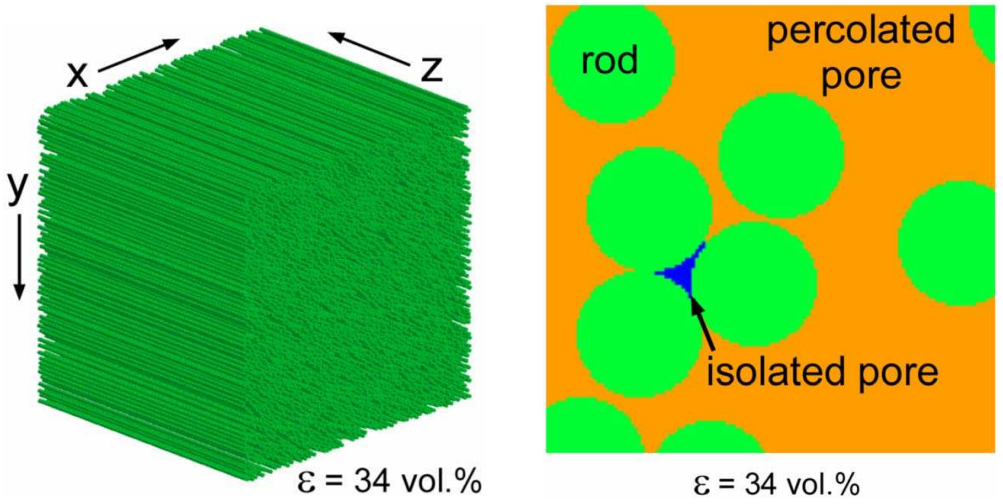

(a) (b)

FIG. 1: Randomly placed parallel rods (green) running in the z-axis. **a)** The x-y plane consists of 3000^2 cubic voxels, and the diameter of each rod is 37 voxels. The pore voxels are transparent. The number of the rods embedded in the image system is 2820. The rod volume fraction, ε, is 34 vol %. **b)** Zoom of (a) viewed from the z-axis. A pore cluster (blue) is completely surrounded by rods (green) and isolated from the percolated pore cluster (orange)

system of the randomly placed pointlike obstacles (not rods) to confirm the validity of the program. The obtained diffusivity value agreed well with that in the literature (Trinh et al., 2000) within an acceptable error. For example, the isotropic diffusivity for the obstacle volume fraction of 50 vol % normalized by that in free space averaged over 200,000 walkers was calculated to be 0.216 by DellipsoidM6.nb; that for the obstacle volume fraction of 30 vol % was 0.535. The literature value for the identical porous system is ~ 0.22 and ~ 0.54, respectively, demonstrating the reliable performance of our program.

The diffusivity along any direction in 3D space is calculated as follows. Each 3D random walk trajectory is projected on the α-axis originating from the center of the 3D image system (Fig. 2). Displacement on the α-axis is used to calculate the walkers' mean square displacement, $\langle \alpha(\tau)^2 \rangle$, in the α direction,

$$\langle \alpha(\tau)^2 \rangle = \frac{1}{n} \sum_{i=1}^{n} \left[\alpha_i(\tau) - \alpha_i(0) \right]^2 \tag{1}$$

where n is the number of random walkers, τ is the dimensionless integer time ($\tau = 0, 1, 2, 3, \ldots$), $\alpha_i(\tau)$ is the coordinate of the walker's position on the α-axis at time τ for the ith walker, and $\alpha_i(0)$ is the initial position of the ith walker. The exact solution for a lattice walk in free space (i.e., porosity = 100 vol %), $\langle \alpha^2 \rangle_{\mathrm{free}}$, is given by $\langle \alpha^2 \rangle_{\mathrm{free}} = \ell^2 \tau / 3$ where ℓ is the lattice constant of the simple cubic lattice (i.e., the dimension of a cubic voxel). The diffusion coefficient is proportional to the time derivative of the mean square displacement (Nakashima and Kamiya, 2007). Normalized diffusivity in the present study refers to the diffusivity in porous media divided by that in free space, and the tortuosity is its reciprocal. Thus, we have

$$\begin{aligned} \text{normalized diffusivity} &= \frac{1}{\text{tortuosity}} \\ &= \frac{d \left\langle \alpha(\tau)^2 \right\rangle / d\tau}{\ell^2 / 3} \quad \text{as} \quad \tau \to \infty \end{aligned} \tag{2}$$

The normalized diffusivity is unity for the random walk in free space, and less than unity for that in porous media owing to the obstructive effect of the solid framework. The asymptote value (i.e., $\tau \to \infty$) is essential because the normalized diffusivity can be overestimated due to the short diffusion distance compared with pore size if the time derivative is taken at a small τ value (Nakashima and Watanabe, 2002). For an identical set of random walk trajectories, the α-axis is systematically scanned on the upper-half plane of the 3D polar coordinate system (Fig. 2) to express the directional mean square displacement as a function of angles θ and ϕ. Equation (2) is again applied to the mean square displacement to obtain the normalized diffusion coefficient depending on θ and ϕ. Typically, θ covers $0, 1, 2, \ldots 90$ deg, and ϕ covers $0, 1, 2, \ldots 359$ deg. Thus, the number of data points obtained for the normalized diffusivity can be as large as $90 \times 360 + 1 = 32,401$, which is usually sufficient to evaluate the diffusive anisotropy of porous media.

The normalized diffusivity, which depends on θ and ϕs can be visualized as a shell-like object by polar representation. Using a diffusion tensor, $\boldsymbol{D}$, we have

$$\text{normalized diffusivity} = \boldsymbol{u}^T \boldsymbol{D} \boldsymbol{u} \tag{3}$$

where $\boldsymbol{u}$ is the unit vector along the α-axis (Frank, 2002). It should be noted that the 3D shape of the shell-like object calculated by Eq. (3) is not exactly identical to the diffusion tensor ellipsoid describing the eigenvectors and eigenvalues of $\boldsymbol{D}$. The nature of the rod packing parallel to the z-axis (Fig. 1) ensures that the shape of the diffusion tensor ellipsoid is a cigar-shaped prolate spheroid. If the stochastic fluctuation is negligible, we have

$$\boldsymbol{D} = \begin{pmatrix} D_{xy} & 0 & 0 \\ 0 & D_{xy} & 0 \\ 0 & 0 & Dz \end{pmatrix} \tag{4}$$

where D_{xy} is the normalized diffusivity on the x-y plane and D_z is the normalized diffusivity in the z direction. The raw data set of the normalized diffusion coefficients calculated by Eq. (2) was fitted to Eq. (3) in terms of the

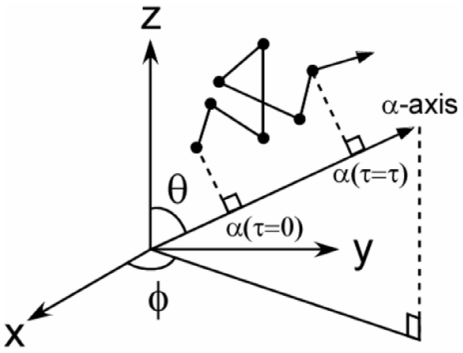

FIG. 2: A random walk trajectory projected on the α-axis originating from the center of the 3D image system to calculate the walkers' mean square displacement in the α direction

second moment of the object as described by Ikeda et al. (2000). First, the search for a principal axis yielding the minimum value of the second moment was performed to assign it to the major axis. Second, a principal axis yielding the maximum value of the second moment (i.e., minor axis) was searched in the direction perpendicular to the major axis. Finally, the third principal axis perpendicular to both the major and minor axes was automatically chosen as the intermediate axis. The crossing points of the shell-like object and the three principle axes were determined to be the eigenvalues of $\boldsymbol{D}$ (i.e., D_{xy} and D_z).

3. RESULTS

Extensive simulations were conducted by systematically varying the rod volume fraction, and the effects of rod volume fraction on the shape and dimensions of the polar representation of the direction-dependent normalized diffusivity were analyzed. Examples of the normalized diffusivity obtained for some values of the rod volume fraction are shown in Fig. 3. This 3D shell-like object is a result of the raw data, and the distances of each point on the shell from the origin are the normalized diffusivity values calculated for 32,401 integer (θ, ϕ) pairs (i.e., $\theta = 0, 1, 2, \ldots 90$ deg and $\phi = 0, 1, 2, \ldots 359$ deg). The number of maximum time steps was $\tau = 300,000$, sufficient to travel a distance relatively long compared with the pore size. The number of the random walkers, n, in Eq. (1) was as large as 400,000 to reduce the undesirable stochastic fluctuation of the mean square displacement. The CPU time of DellipsoidM6.nb required for calculation of each ellipsoid was 5.9 h using a personal computer (PC) with an Intel Core2 Duo T7600 CPU (2.33 GHz) and 2 GB RAM running Windows XP. Theoretically, the ellipsoid for $\varepsilon = 0$ vol % (i.e., free space) should be a complete sphere with a radius of unity. Figure 3 shows that the fitted major, intermediate, and minor principal values of the normalized diffusivity averaged over 400,000 walkers were 1.016, 1.006, and 1.001, respectively. These are very close to the theoretical value of unity, demonstrating that our random walk simulations were performed reliably.

Figure 3 clearly shows that the shape of the direction-dependent normalized diffusivity becomes prolate in the z direction for nonzero ε values. This prolate nature is a consequence of the pore structure being less tortuous in the longitudinal direction of the rod and more tortuous in the x-y direction. Note that in Fig. 3 the shape of the normalized diffusivity is no longer convex ellipsoidal for a large ε value, but is constricted in the x-y direction. The constriction is also found for highly anisotropic fibrous porous media (Frank, 2002; Nakashima et al., 2008). The occurrence of the constriction is a main focus of the present study, and results of detailed analysis are shown in Figs. 4–6.

Figure 4 shows the full set of lattice walk simulation outputs for $\varepsilon = 51$ vol % of Fig. 3. The mean square displacements along the x-, y-, and z-axes indicated in Fig. 1a, as calculated by Eq. (1), are shown in Fig. 4a. Equation (1) becomes simple if the cubic voxel dimension, ℓ, is unity. Thus, $\ell = 1$ was assumed in

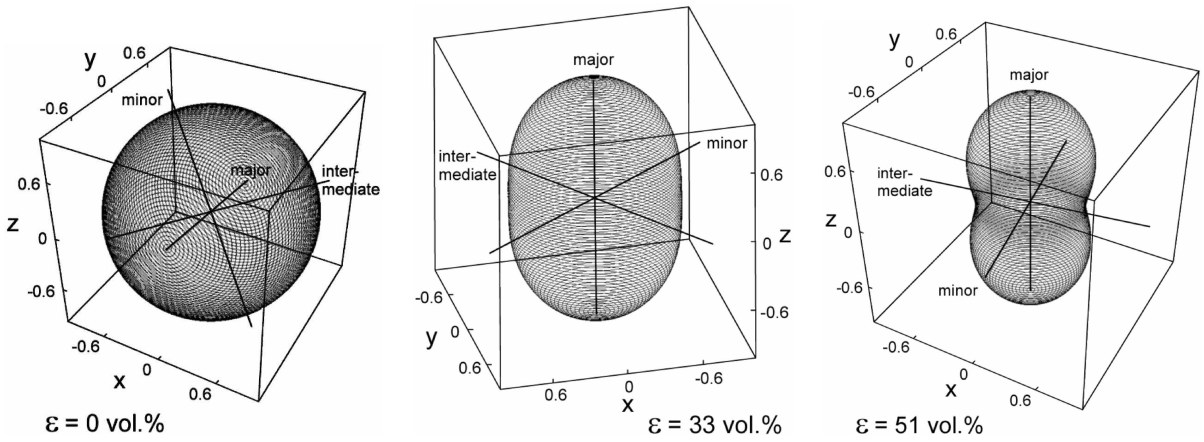

FIG. 3: View from above of the wireframe rendering of normalized diffusivity calculated by Eq. (2) for three values of rod fraction ε. The dimension of the whole image system and rod diameter value are identical to those in Fig. 1. The three principal axes are superimposed

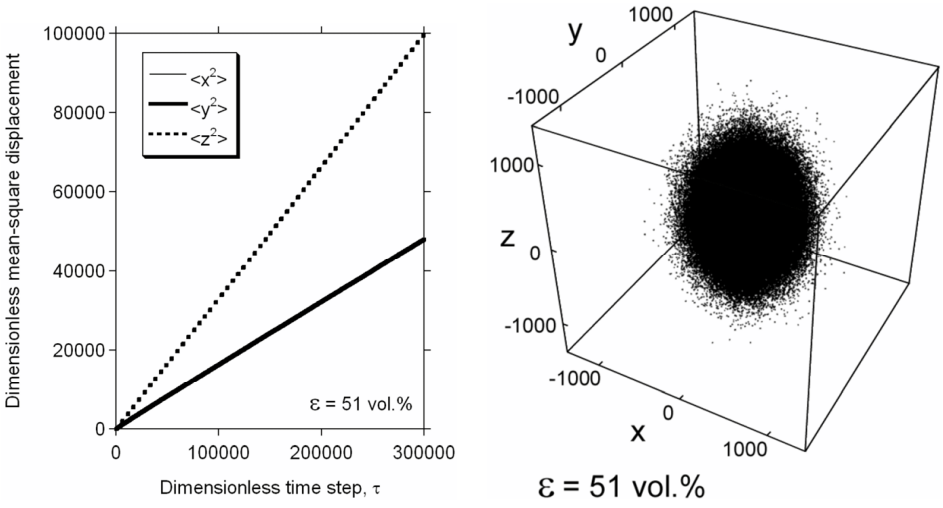

(a) (b)

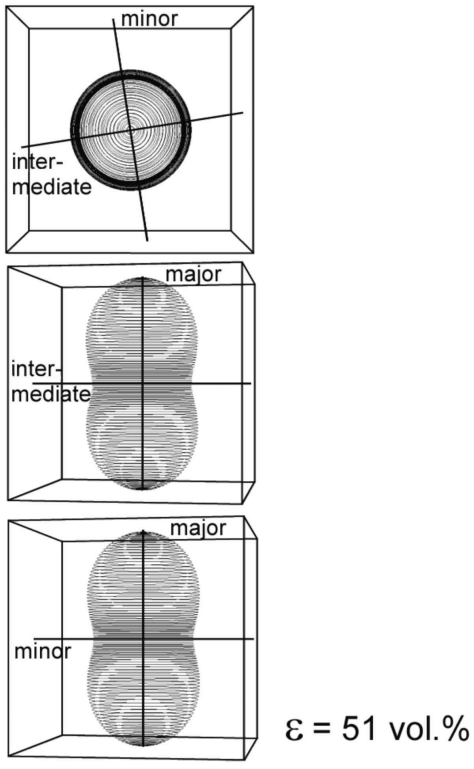

(c)

FIG. 4: Detailed results of a random walk simulation for $\varepsilon = 51$ vol %. **a)** Dimensionless mean square displacement along the x-, y-, and z-axes averaged over 400,000 walkers. **b)** Snapshot of 400,000 walkers at $\tau = 300,000$. **c)** Wireframe rendering of the normalized diffusivity viewed along the three principal axes

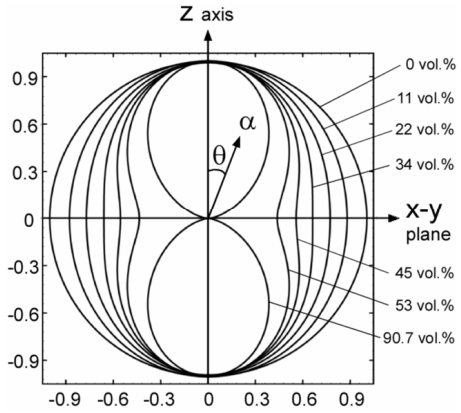

FIG. 5: Two-dimensional polar representation of normalized diffusivity for various values of rod volume fraction ε (in vol %). Normalized diffusivity for the hexagonal closest rod packing of $\varepsilon = \pi/(12)^{0.5} \sim 90.7$ vol % and that for Eq. (5) also are plotted, but it is difficult to distinguish between them with this image resolution

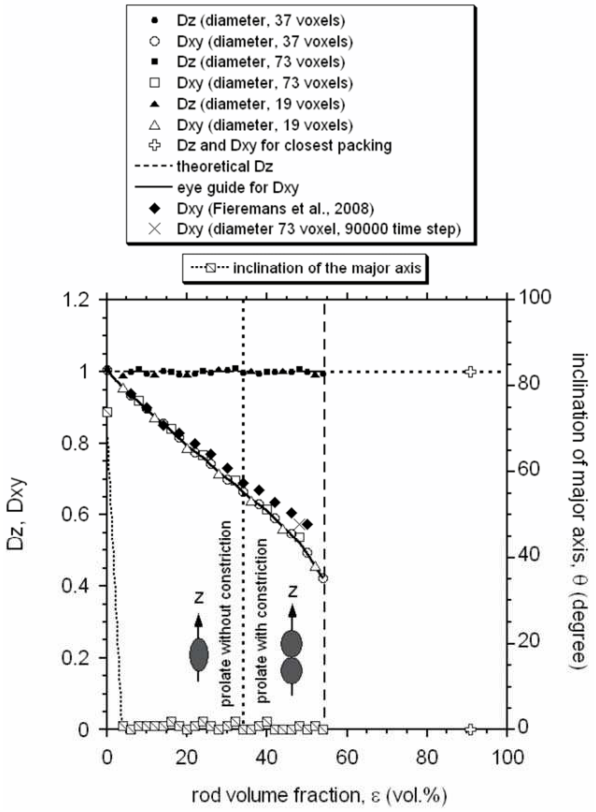

FIG. 6: Eigenvalues [i.e., D_{xy} and D_z of Eq. (4)] and major axis inclinations as a function of rod volume fraction, ε. The solid line was placed as a guide. The two regimes with a boundary (vertical dotted line) of $\varepsilon = 34$ vol % are illustrated. The theoretical value for D_z is shown by a horizontal dotted line ($D_z = 1$). The upper bound of ε for the random sequential rod packing by Tanemura (1988) is indicated by a vertical broken line ($\varepsilon \sim 54.7$ vol %). Theoretical values for the hexagonal closest packing of parallel rods also are indicated by $D_z = 1$ and $D_{xy} = 0$ at $\varepsilon = \pi/(12)^{0.5} \sim 90.7$ vol %

Fig. 4a, yielding a dimensionless mean square displacement. The mean square displacement in the z direction is significantly larger than those in the x and y directions, and quantities $\langle x^2 \rangle$ and $\langle y^2 \rangle$ are indistinguishable, implying that the shape of the direction-dependent normalized diffusivity is a cigar-shaped prolate spheroid. To avoid an undesirable overestimate of the normalized diffusivity due to a short diffusion distance compared with pore size (Nakashima and Kamiya, 2007), a sufficiently large value (as large as 300,000) was employed for the random walk time step to obtain linear (not convex) mean square displacement. As a result, the convex portion of the mean square displacement curve is limited in the very early stage (i.e., $\tau < 10000$). This time interval with a convex mean square displacement should be eliminated from the calculation of normalized diffusivity because the time derivative [Eq. (2)] has not yet reached the asymptote value. Thus, to obtain a reliable diffusion ellipsoid, the time derivative was calculated using the very last portion of the mean square displacement time series data for all simulations of the present study, namely, the slope value of $\langle \alpha(\tau)^2 \rangle$ between the maximum time step and 75% of it was employed. For example, the normalized diffusivity was calculated using the difference of $\langle \alpha(\tau)^2 \rangle$ at $\tau = 300,000$ and $300,000 \times 0.75 = 225,000$ for Fig. 4a. The final positions of all the walkers are shown in Fig. 4b. The origin of the 3D image is the starting position of each walker. The unit of the axes is the cubic voxel dimension, ℓ. Figure 4b is the diffusion front, showing again the cigar-shaped prolate spheroid. This was confirmed by the ellipsoid fitting result that inclination θ of the ellipsoid major axis was as small as 0 deg with $D_{xy} = 0.47$ and $D_z = 1.01$, clearly indicating that the direction-dependent normalized diffusivity is a prolate spheroid and the elongation direction was parallel to the z-axis. The prolate shape can be seen more clearly when viewed from the principal axes (Fig. 4d). Particularly when viewed from the minor and intermediate axes, the unusual shape constricted in the direction normal to the major axis is obvious.

The onset of the constriction was investigated in detail by calculating the shape of the 3D shell-like object of the normalized diffusivity for various values of rod volume fraction, ε. The number of walkers, the maximum time step, dimension of the whole image system, and rod diameter are identical to those in Figs. 1, 3, and 4. The longitudinal direction of the parallel rods lies along the z direction (Fig. 1). Therefore, the normalized diffusivity for the fibrous system should be independent of ϕ (i.e., symmetric with respect to the z-axis). Thus, it is reasonable to average the normalized diffusivity over $\phi = 0$ to 359 deg at a specified θ value. The averaged cross section of the shell-like object (Fig. 5) obtained is θ dependent only, and clearly shows that the isotropic circle for $\varepsilon = 0$ vol % becomes prolate as the ε value increases. It should be noted that when the ε value exceeds the critical value of 34 vol %, constriction of the polar representation of the normalized diffusivity appears in the direction of minimum diffusivity (i.e., in the direction of $\theta = 90$ deg). This constriction becomes most evident for the hexagonal closest rod packing status (Tóth, 1972) of $\varepsilon = \pi/(12)^{0.5} \sim 90.7$ vol %.

Effects of ε on D_{xy} and D_z are summarized in Fig. 6. TheD_{xy} value is the normalized diffusivity averaged on the x-y plane (i.e., normalized diffusivity averaged over $\phi = 0$ to 359 deg at $\theta = 90$ deg), while D_z is the normalized diffusivity in the z direction (i.e., normalized diffusivity for $\theta = 0$ deg). Theoretically, D_{xy} and D_z should be dependent only on ε and independent of rod diameter, which is confirmed by Fig. 6. The value of D_{xy} decreases with increasing ε while D_z remains constant. The tortuosity normal to the z-axis increases with rod fraction because the rods act as obstacles for the random walkers. This mechanism is responsible for the decrease in D_{xy} with increasing ε Because all rods are completely in parallel, no obstruction exists for walkers migrating in the z-axis. As a result, the tortuosity along the z-axis is identical to that in free space, and D_z remains unity, as shown in Fig. 6.

The cigar-shaped prolate spheroid of the direction-dependent diffusivity for the fibrous system in Fig. 1 is symmetric with respect to the z-axis. Therefore, the inclination, θ of the major axis of spheroid should be 0 deg The calculated inclination of the major axis is shown in Fig. 6. Although a slight discrepancy from 0 deg exists that is derived from the stochastic nature of the pseudo-random number generator used in the random rod packing and lattice random walk, Fig. 6 shows that $\theta \sim 0$ deg. This demonstrates that our random walk simulations were performed successfully.

Fieremans et al. (2008) performed diffusion simulations in randomly packed parallel rods. Although they did not analyze the constriction of the 3D shape of the direction-dependent diffusivity, some D_{xy} values have been reported and incorporated in Fig. 6. The results by Fieremans et al. (2008) agree approximately with the present study. However, there is a slight discrepancy, particularly for $\varepsilon > 40$ vol %. The discrepancy is probably derived from the difference of the diffusion distance of the random walkers. To save computation time, Fieremans et

al. (2008) performed short-distance simulations that the ratio of the diffusion distance in the x-y plane to the rod diameter was as small as 2.5, and predicted the asymptote (i.e., $\tau \rightarrow \infty$) tortuosity value using the two-point Padé approximation, which yields a worse fit for high ε values. In contrast, we have performed long-distance random walk (typically the ratio of the diffusion distance to the rod diameter was ~ 10). A D_{xy} value of 0.573 for a 90,000 time step (the ratio was ~ 2.5) obtained by DellipsoidM6.nb simulation is plotted for $\varepsilon = 48$ vol %. The obtained D_{xy} value is significantly larger than the D_{xy} value of 0.537 obtained by a long-distance (the ratio was ~ 18) simulation as plotted in Fig. 6, and lies on the trend of the data points by Fieremans et al. (2008). This supports the interpretation described above for the discrepancy of the D_{xy} values.

Theoretically, $D_z = 1$ for $\varepsilon \leq \sim 90.7$ vol % because a random walk in the z direction is identical to that in free space. There is a slight fluctuation in the 27 D_z values plotted in Fig. 6 derived from the stochastic nature of the pseudorandom number generator. According to a statistical analysis of the 27 data points, the average of D_z was 1.00004, very close to the theoretical value of unity, and the standard deviation normalized by the theoretical value was as small as 0.5 %, indicating acceptable accuracy and precision of the computer simulations.

4. DISCUSSION

Lattice random walk simulations were conducted in the randomly packed rod system shown in Fig. 1. Results confirmed that the direction-dependent normalized diffusivity is prolate in the longitudinal direction of the parallel rods. The distortion of the ellipsoidal shape was calculated by systematically changing values for the rod volume fraction, ε. The results are summarized in Figs. 3–6, and show that diffusivity normal to the longitudinal direction decreases with increasing ε due to obstruction of the impermeable parallel rods while diffusivity along the longitudinal direction remained constant. The parallel rod system examined in the present study is a model for fibrous porous media that are commonly found in many fields such as biology, material engineering, and geology. Therefore, the quantitative behavior of the direction-dependent normalized diffusivity (Figs. 3–6) is useful to estimate the diffusive transport properties in real fibrous porous media found in such diverse fields.

Systematic simulations for varied rod volume fractions revealed that the 3D shape of the polar representation of the direction-dependent normalized diffusivity was no longer convex ellipsoidal, but was constricted in the direction normal to the rod axis when the rod volume fraction exceeded 34 vol % (Fig. 5). This study is the first report that constriction of the direction-dependent diffusivity occurs in a randomly packed parallel rod system, a very simple model system having a unidirectional pore structure. To understand the nature of the constriction, an exact solution of the direction-dependent self-diffusivity with constriction was presented for the lattice walk in a straight pore. A lattice walk in a straight pore cluster embedded in a solid (Fig. 7) is a simple but effective model to examine the diffusion in fibrous porous media. Random walkers diffuse in the straight pore cluster by colliding against the wall. Walker motion is completely restricted in the x and y directions, and completely free in the z direction. The resultant mean square displacement along the z-axis, $\langle z(\tau)^2 \rangle$, is $\ell^2\tau/3$ (Nakashima and Kamiya, 2007). When the unidirectional random walk trajectory is projected on the α-axis (Fig. 2) with inclination θ, the unit length ℓ should be replaced with $\ell \cos\theta$. Substituting $\langle \alpha(\tau)^2 \rangle = (\ell \cos\theta)^2 \tau/3$ into Eq. (2) gives

$$\text{normalized} \quad \text{diffusivity} = \cos^2\theta \tag{5}$$

The 3D shape is obtained by rotating Eq. (4) with respect to the z-axis. Equation (5) is plotted in Fig. 5, clearly showing the ellipsoid constriction in the direction

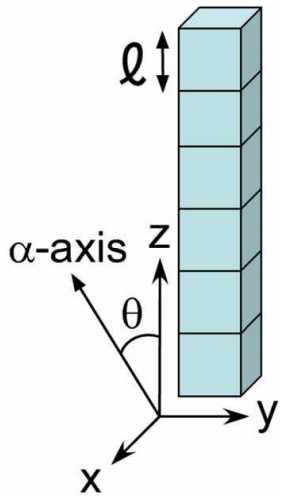

FIG. 7: Straight pore cluster embedded in a solid as an example of strongly anisotropic 3D fibrous porous media. The longitudinal length of the cluster in the z-axis is infinite, and the cross-sectional area is ℓ^2 where ℓ is the cubic voxel dimension

of $\theta = 90$ deg. It is difficult to distinguish Eq. (5) from the normalized diffusivity calculated for the hexagonal closest packing of parallel rods (Fig. 5). Thus, it is reasonable to take that Eq. (5) is for an end member of the densely packed rod system. The mechanism of onset of the constriction can then be explained as follows. Diffusion in the randomly placed rod system is a *mixture* (not a mechanical mixture) of the two end members: isotropic diffusion in free space ($\varepsilon = 0$ vol %) and highly anisotropic diffusion in the hexagonal closest packing ($\varepsilon \sim 90.7$ vol %). For a system with a relatively low ε value, the contribution of the former is dominant, and the constriction by the latter end member is masked, yielding a cigar-shaped prolate spheroid without constriction. In contrast, for a system with an ε value of > 34 vol %, the contribution of Eq. (5) becomes dominant, eliminating the convex nature of the prolate spheroid and producing the constriction in the $\theta = 90$ deg direction. Thus, the constriction of the 3D shape of the direction-dependent normalized diffusivity observed for randomly placed parallel rods is a *remnant* of the hexagonal closest packing status.

As shown in Figs. 5 and 6, the onset of the constriction of the prolate spheroid at $\varepsilon = 34$ vol % corresponds to $D_z/D_{xy} = 1/0.664$, which is ~ 1.5. To elucidate the onset mechanism of the constriction at $D_z/D_{xy} \sim 1.5$, the following analysis was performed. Consider two-dimensional anisotropic diffusion in the x-z plane for simplicity (Fig. 8). The direction-dependent normalized diffusivity is given by Eq. (3) where $\boldsymbol{u} = (\cos\delta, \sin\delta)$ and δ is the complementary angle of θ. The corresponding diffusion tensor is

$$\boldsymbol{D} = \begin{pmatrix} D_x & 0 \\ 0 & Dz \end{pmatrix} \tag{6}$$

where $D_z > D_x$. On the marginal or neutral condition, the shape of the polar representation of the direction-dependent diffusivity is straight near the x-axis. This indicates that OAB in Fig. 8 is a right-angled triangle and yields $\mathrm{OB} \times \cos\delta = \mathrm{OA}$ for $\delta \ll 1$. Substituting Eq. (3) into OB and OA for $\cos\delta \approx 1 - \delta^2/2$ and $\sin\delta \approx \delta$, we have

$$\left(D_z - \frac{3}{2}D_x\right)\delta^2 + o(\delta^4) = 0 \tag{7}$$

Equation (7) indicates that the constriction of the cigar-shaped prolate spheroid occurs when D_z/D_x exceeds exactly 1.5, which agrees well with the 3D simulation results of Figs. 5 and 6. It is straightforward to examine to the constriction of disk-shaped oblate spheroid (i.e., $D_z < D_x$) using the similar formulation to obtain the critical value of $D_z/D_x = 2/3$ (i.e., reciprocal of 1.5) with respect to the onset of the constriction for the oblate spheroid.

Nakashima et al. (2008) performed random walk simulations for natural anisotropic porous rocks, and found that the constriction of the prolate-oblate diffusion ellipsoids occurred when the maximum-to-minimum diffusivity ratio of the direction-dependent diffusivity exceeded ~ 1.5. An oblate (not prolate) diffusion ellipsoid with constriction has been observed for water self-diffusion in discoidal clay gels when $D_z/D_x \approx 2/3$ using nuclear magnetic resonance spectroscopy (Porion et al., 2001). It is noteworthy that the critical value of 1.5 (or its reciprocal, 2/3) is common among the rod packing system, natural rocks, and clay gels even though the pore structure of the synthetic system of parallel rods (Fig. 1) and that of natural rocks/gels are quite different.

Anisotropic thermal conductivity is one of some important subjects for fibrous porous media (Tien and Vafai, 1979). The thermal conduction phenomenon obeys a parabolic partial differential equation as well as the material diffusion phenomenon. Thus, the present study predicts that constriction of the 3D shape of the direction-dependent thermal diffusivity also would occur if the material possesses high anisotropy with respect to thermal conductivity. Examples include anisotropic porous metals composed of conductive metal and less conductive elongated gas-filled pores (Nakajima, 2007).

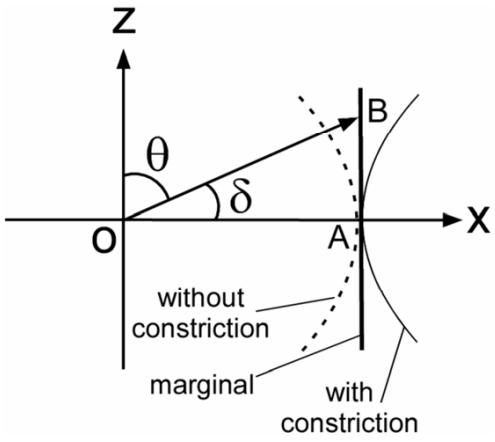

FIG. 8: Two-dimensional schematic of the shape of the direction-dependent normalized diffusivity curves near the x-axis. Three curves (concave, convex, and straight) are for the with-, without-constriction, and marginal cases, respectively

5. CONCLUSIONS

To understand the process of diffusion in anisotropic fibrous porous media, lattice random walk simulations in a model system consisting of randomly packed parallel rods were performed. Results showed that the direction-dependent normalized diffusivity obtained was prolate in the longitudinal direction of the parallel rods. This is a consequence of the anisotropic pore structure of the rod system that enables high diffusive migration along the longitudinal direction. Systematic simulations for varied packing densities revealed that the cigar-shaped prolate spheroid loses its convex nature, but becomes constricted in the direction normal to the rod axis when the maximum-to-minimum diffusivity ratio of the diffusion ellipsoid exceeds ~ 1.5. An analytical solution of the direction-dependent diffusivity with constriction was presented for a random walk in a straight pore. The solution suggested that the constriction observed for the randomly placed parallel rods is a *remnant* of the anisotropic pore structure of the hexagonal closest packing, which is the end member of the rod packing. The onset condition of the constriction of the shape of the direction-dependent diffusivity was investigated analytically using a diffusion tensor expression. The analysis revealed that the constriction occurs when the maximum-to-minimum diffusivity ratio exceeds exactly 1.5, which agrees well with the simulation results. The critical value of 1.5 can also be applicable to the geologically deformed natural porous rocks having more complex pore structure compared with the simple rod packing system.

ACKNOWLEDGMENTS

Comments by three anonymous reviewers were helpful. This study was partially supported by METI of the Japanese government.

REFERENCES

Fieremans, E., De Deene, Y., Delputte, S., Özdemir, M. S., D'Asseler, Y., Vlassenbroeck, J., Deblaere, K., Achten, E., and Lemahieu, I., Simulation and experimental verification of the diffusion in an anisotropic fiber phantom, *J. Magn. Reson.*, vol. **190**, pp. 189–199, 2008.

Frank, L. R., Characterization of anisotropy in high angular resolution diffusion-weighted MRI, *Magn. Reson. Med.*, vol. **47**, pp. 1083–1099, 2002.

Guild, F. J. and Summerscales, J., Microstructural image-analysis applied to fiber-composite materials—A review, *Composites*, vol. **24**, pp. 383–393, 1993.

Ikeda, S., Nakano, T., and Nakashima, Y., Three-dimensional study on the interconnection and shape of crystals in a graphic granite by x-ray CT and image analysis, *Miner. Mag.*, vol. **64**, pp. 945–959, 2000.

Jian, B., Vemuri, B. C., Özarslan, E., Carney, P. R., and Mareci, T. H., A novel tensor distribution model for the diffusion-weighted MR signal, *Neuroimage*, vol. **37**, pp. 164–176, 2007.

Matsumoto, M. and Nishimura, T., Mersenne twister: A 623-dimensionally equidistributed uniform pseudorandom number generator, *ACM Trans. Model. Comput. Simul.*, vol. **8**, pp. 3–30, 1998.

Nakajima, H., Fabrication, properties and application of porous metals with directional pores, *Prog. Mater. Sci.*, vol. **52**, pp. 1091–1173, 2007.

Nakashima, Y. and Kamiya, S., Mathematica Programs for the analysis of three-dimensional pore connectivity and anisotropic tortuosity of porous rocks using x-ray computed tomography image data, *J. Nucl. Sci. Technol.*, vol. **44**, pp. 1233–1247, 2007.

Nakashima, Y. and Watanabe, Y., Estimate of transport properties of porous media by micro-focus x-ray computed tomography and random walk simulation, *Water Resour. Res.* 1272, vol. **38**, 2002.

Nakashima, Y., Kamiya, S., and Nakano, T., Diffusion ellipsoids of anisotropic porous rocks calculated by x-ray computed tomography-based random walk simulations, *Water Resour. Res.* W12435, vol. **44**, 2008.

Nakashima, Y., Nakano, T., Nakamura, K., Uesugi, K., Tsuchiyama, A., and Ikeda, S., Three-dimensional diffusion of non-sorbing species in porous sandstone: Computer simulation based on x-ray microtomography using synchrotron radiation, *J. Contam. Hydrol.*, vol. **74**, pp. 253–264, 2004.

Porion, P., Rodts, S., Al-Mukhtar, M., Faugére, A. M., and Delville, A., Anisotropy of the solvent self-diffusion tensor as a probe of nematic ordering within dispersions of nanocomposites, *Phys. Rev. Lett.* 208302, vol. **87**, 2001.

Sen, P. N. and Basser, P. J., A model for diffusion in white matter in the brain, *Biophys. J.*, vol. **89**, pp. 2927–2938, 2005.

Tanemura, M., Random packing and random tessellation in relation to the dimension of space, *J. Microsc.-Oxf.*, vol. **151**, pp. 247–255, 1988.

Teshima, Y., Watanabe, Y., and Ogawa, T., A new structure of cylinder packing, *Discret. Comput. Geom. (Lecture Notes Comput. Sci.)*, vol. **2098**, pp. 351–361, 2001.

Tien, C. L. and Vafai, K., *Statistical Bounds for the Effective Thermal Conductivity of Microsphere and Fibrous Insulation*, AIAA Progress Series, vol. **65**, pp. 135–148, AIAA, Washington, DC, 1979.

Tóth, L. F., *Lagerungen in der Ebene, auf der Kugel und im Raum*, Springer, Heidelberg, 1972.

Trinh, S., Arce, P., and Locke, B. R., Effective diffusivities of point-like molecules in isotropic porous media by monte carlo simulation, *Transp. Porous Media*, vol. **38**, pp. 241–259, 2000.